# Effect of radial location of nozzles on performance of preswirl systems: a computational and theoretical study

**P Lewis, M Wilson*, G D Lock,** and **J M Owen**
Department of Mechanical Engineering, University of Bath, UK

*The manuscript was received on 4 September 2008 and was accepted after revision for publication on 20 November 2008.*

DOI: 10.1243/09576509JPE689

**Abstract:** This article investigates the effect of the radial location of the inlet nozzles on the performance of a direct-transfer preswirl system in a rotor–stator wheel-space. A commercial code is used to solve the Reynolds averaged Navier–Stokes equations using a high-Reynolds-number $k-\varepsilon/k-\omega$ turbulence model with wall functions. The three-dimensional steady-state model has previously been validated against experimental results from a scale model of a gas turbine rotor–stator system. Computations are performed for three inlet-to-outlet radius ratios, $r_\mathrm{p}/r_\mathrm{b} = 0.8$, 0.9, and 1.0, a range of preswirl ratios, $0.5 < \beta_b < 2.0$, and varying turbulent flow parameters, $0.12 < \lambda_T < 0.36$. The rotational Reynolds number for each case is $10^6$.

The flow structure in the wheel-space and in the region around the receiver holes for each inlet radius is related to the swirl ratio. The performance of the system is quantified by two parameters: the discharge coefficient for the receiver holes ($C_\mathrm{d,b}$) and the adiabatic effectiveness for the system ($\Theta_\mathrm{b,ad}$).

As in previous work, the discharge coefficient is found to reach a maximum when the rotating core of fluid is in synchronous rotation with the receiver holes. As the radius ratio is increased, this condition can be achieved with a smaller value for preswirl ratio $\beta_\mathrm{b}$. A simple model is presented to estimate the discharge coefficient based on the flowrate and swirl ratio in the system.

The adiabatic effectiveness of the system increases linearly with preswirl ratio but is independent of flowrate. For a given preswirl ratio, the effectiveness increases as the radius ratio increases. Computed values show good agreement with analytical results. Both performance parameters show improvement with increasing inlet radius ratio, suggesting that for an optimum preswirl configuration an engine designer would place the preswirl nozzles at a high radius.

**Keywords:** computational fluid dynamics, discharge coefficients, gas turbines

## 1 INTRODUCTION

A simplified diagram of the so-called direct-transfer preswirl system, where the blade-cooling air is supplied to the rotating blades by stationary angled preswirl nozzles, is shown in Fig. 1. The nozzles swirl the air, and this reduces the work done by the rotating turbine disc in accelerating the air to the disc speed. This consequently reduces the total temperature of the air entering the receiver holes in the disc [**1**]. The designer is interested in calculating the pressure drop and cooling effectiveness of the preswirl system, and there is also a need to understand the heat transfer between the cooling air and the turbine disc.

Heat transfer in a direct transfer rig was studied experimentally and computationally by Wilson *et al.* [**2**]. Total temperature probes were used to measure the temperature of the air entering the receiver holes, which was consistently underpredicted by axisymmetric computational fluid dynamics (CFD) computations.

Geis *et al.* [**3**] made measurements of adiabatic effectiveness, which showed that the measured values of $T_\mathrm{t,b}$, the total temperature of the air in the rotating frame of reference entering the receiver holes, were significantly higher than the values predicted from their ideal model. Chew *et al.* [**4**] made numerical simulations that were in good agreement with results from

**Corresponding author: Department of Mechanical Engineering, University of Bath, Bath, BA2 7AY, UK. email: ensmw@bath.ac.uk*

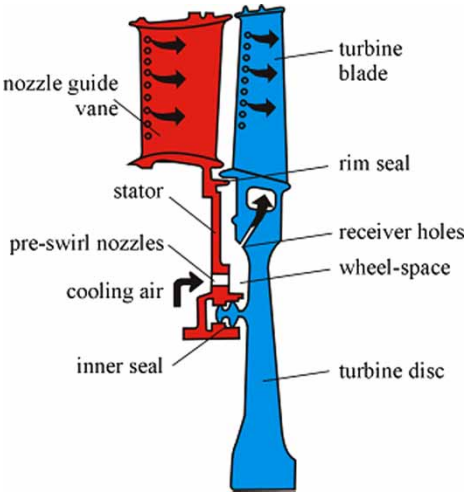


**Fig. 1** Simplified diagram of a direct-transfer preswirl system

both the 'Karlsruhe' preswirl rig used by Geis *et al.* and a preswirl rig at Sussex University. Chew *et al.* and Farzaneh-Gord *et al.* [**5**] derived independently theoretical models for the adiabatic effectiveness.

Dittmann *et al.* [**6**] measured the discharge coefficients for the preswirl nozzles and receiver holes in a direct-transfer system, and Yan *et al.* [**7**] measured the discharge coefficients for receiver holes. Lewis *et al.* [**8**] carried out a combined computational and experimental study of a direct-transfer system. The computed adiabatic effectiveness was in good agreement with the theoretical expression derived by Farzaneh-Gord *et al.*, and the computed values of $C_{\mathrm{d,b}}$, the discharge coefficient for the receiver holes, reached a maximum value at a critical value of $\beta_{\mathrm{p}}$, the preswirl ratio of the cooling air.

Lewis *et al.* studied a system having the preswirl inlet at a lower radius than that of the receiver holes (as illustrated in Fig. 1), while the Karlsruhe rig used by Dittman *et al.* involved preswirl nozzles and receiver holes at the same high radius. Jarzombek *et al.* [**9**] computationally studied a configuration with the preswirl nozzles located radially outward of the receiver holes, finding the flow to conform to free vortex behaviour. It is the objective of the present article to determine the effect of the radial location of the preswirl nozzles on system performance.

In previous papers by the authors, in which only one location for the preswirl nozzles was considered, the preswirl ratio $\beta_{\mathrm{p}}$ was defined as the ratio of the tangential velocity of the air at the preswirl inlet to the disc speed at the preswirl radius

$$\beta_{\mathrm{p}} = V_{\phi,\mathrm{p}}/\Omega r_{\mathrm{p}} \tag{1}$$

In an engine, the total pressure upstream of the preswirl nozzles is fixed. If the static pressure in the core was also fixed, then the preswirl velocity $V_{\phi,\mathrm{p}}$ would be invariant with radius. Under these conditions, it is convenient to define a new preswirl ratio, $\beta_{\mathrm{b}}$ say, where

$$\beta_{\mathrm{b}} = V_{\phi,\mathrm{p}}/\Omega r_{\mathrm{b}} \tag{2}$$

i.e. where the disc speed at the receiver hole radius is used as the reference so that $\beta_{\mathrm{b}}$ is invariant with $r_{\mathrm{p}}$, which is the assumption made for the computations presented below. This will make it easier to identify the effect of nozzle location on preswirl performance. (As shown in Appendix 2, the static pressure in the core does vary with radius, and this has an effect on $\beta_{\mathrm{b}}$ that reduces, but does not negate, the advantages of locating the preswirl nozzles at as high a radius as practicable.)

The computational method is described below, and subsequent sections consider the effect of nozzle location on the flow structure, the discharge coefficient for the receiver holes, the pressure drop in the system, and the adiabatic effectiveness.

## 2 COMPUTATIONAL METHOD

The computational method and configuration are similar to that described in Lewis *et al.* [**8**], with adjustments made for multiple inlets; the salient details are included here for completeness. The computational domain, Fig. 2, is a 6° section of a wheel-space bounded by a rotor and a stator disc with axial gap ratio $G = 0.051$. Cyclic symmetry is imposed at the circumferential boundaries. The system is sealed at its periphery (where $b = 0.216$ m) by a shroud attached to each disc, and the centre of the system is sealed by a stationary hub. Clearances between rotating and stationary surfaces are set to zero.

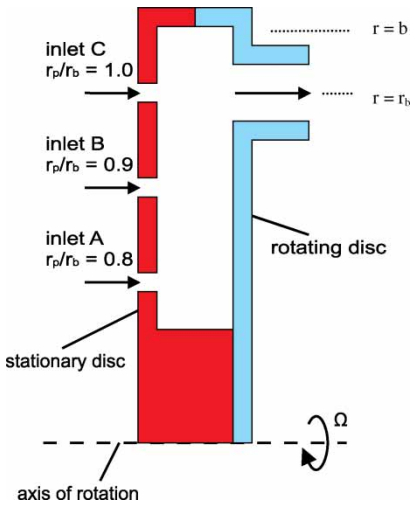


**Fig. 2** Schematic diagram of the flow domain used for the computational study

A cylinder, representing the blade cooling passage, of diameter 8 mm and length 10 mm is attached to the rotor at a radius $r_b = 0.200$ m and rotates with the disc. The preswirl nozzles are represented by an annular slot that can be placed at one of the three radial locations such that $r_p/r_b = 0.8$, 0.9, or 1.0. The height of the annular slot is adjusted so that the preswirl inlet area remains the same at each of these three radial locations. The same set of values for the turbulent flow parameter, in the range $0.12 < \lambda_T = c_w Re_\phi^{-0.8} < 0.36$, is used for each configuration, and the preswirl ratio $\beta_b$ is varied as a parameter. The turbulent flow parameter combines the effects of flowrate and rotational speed in characterizing the flow found in rotor–stator systems [**10**]; for fixed rotational Reynolds number $\lambda_T$ varies with non-dimensional mass flowrate $c_w$. The rotational Reynolds number considered here is $Re_\phi = 10^6$ (corresponding to a rotor disc speed of 3800 r/min). This is lower than the values expected in engines; however, the values of $\lambda_T$ used are representative of engine conditions. Yan *et al.* [**7**] among others have shown that it is the value of $\lambda_T$ rather than $Re_\phi$ that determines the flow structure.

The surface mesh for the geometry is created using a Delaunay triangulation with prismatic elements near the boundaries for better near-wall resolution. An advancing front mesher is then used to resolve the volume. Grid refinement tests were conducted and it was found that flow structure and velocity magnitudes achieved convergence using a mesh size containing ≈810 000 cells.

CFX-10, a commercial three-dimensional finite-volume multi-grid computational fluid dynamics package is used to solve the Reynolds-averaged Navier–Stokes equations. The second-order accurate advection scheme is based on the method of Barth and Jesperson [**11**]. The energy equation is solved including the viscous work term, and the effects of variable density are taken into account. Gravitational buoyancy effects within the wheel-space are ignored.

The turbulence model used is the high-Reynolds-number BSL (BaSeLine) model of Menter [**12**]. This is a blend of a $k-\omega$ formulation with wall functions in the near-wall region, Wilcox [**13**], and a $k-\varepsilon$ model away from the wall. This gives rise to generally reduced turbulence levels compared with $k-\varepsilon$ models and overcomes sensitivities to free stream turbulence levels experienced by $k-\omega$ models. The model was found by the authors to give improved predictions of measured velocity distributions in rotor–stator flows compared with $k-\varepsilon$ models. Other workers (for example, Evans *et al.* [**14**], using the closely related SST model) have reached similar conclusions.

The equations were solved in the rotating frame such that a steady-state analysis could be used. Axial and circumferential velocities were specified at the annular slot being used for the inlet. The two remaining slots in each analysis were treated as part of the solid stator. A static pressure boundary condition was used at the outlet. A normalized total residual convergence criteria of $10^{-7}$ was used for each variable, and velocities were monitored at points within the flow to ensure that a converged state of the flow structure had been obtained.

## 3 FLOW STRUCTURE

The computed flow structure in the radial ($r-z$) plane for typical flowrates and preswirl ratios is shown in Fig. 3(a), (b), and (c) for the case where the inlet is located at $r_p/r_b = 0.8, 0.9$, and 1.0, respectively. The circumferential location $\phi$ of the plane shown coincides with the centre-line of the receiver hole. (There is little effect of circumferential location on the flow structure except in the immediate region of the receiver hole.) For $r_p/r_b = 0.8$ the inlet flow impinges upon the rotating disc and travels radially outwards, forming the rotor boundary layer. Radial inflow occurs on the stator and a pair of counter-rotating vortices can be observed inboard of the inlet.

As the inlet is moved radially outwards, the circulation in the outer part of the system becomes more compressed. The pair of counter-rotating vortices inward of the inlet expands to fill the available space, the larger of the two vortices being that with outflow on the rotor.

The flow is most complex for the case when $r_p/r_b$ is unity (see Fig. 3(c)). Some of the inlet flow enters the receiver holes directly, while the remaining flow impinges upon the region between the holes. The impinging flow spreads both radially inwards and radially outwards from the impingement region. The inward flow encounters the rotor boundary layer flow and separates from the disc, creating the small recirculation on the rotor side inward of the receiver hole.

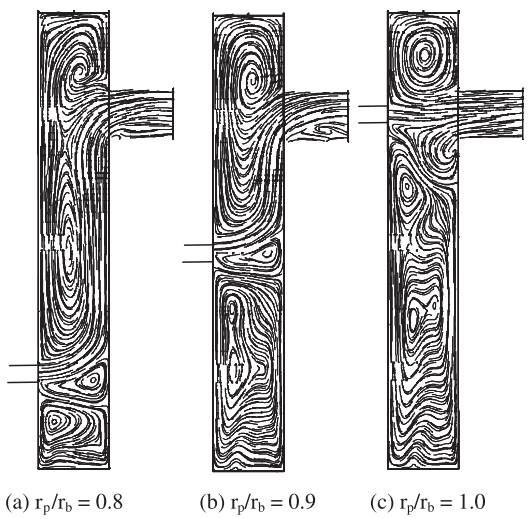


**Fig. 3** Computed flowfields in the axial–radial plane

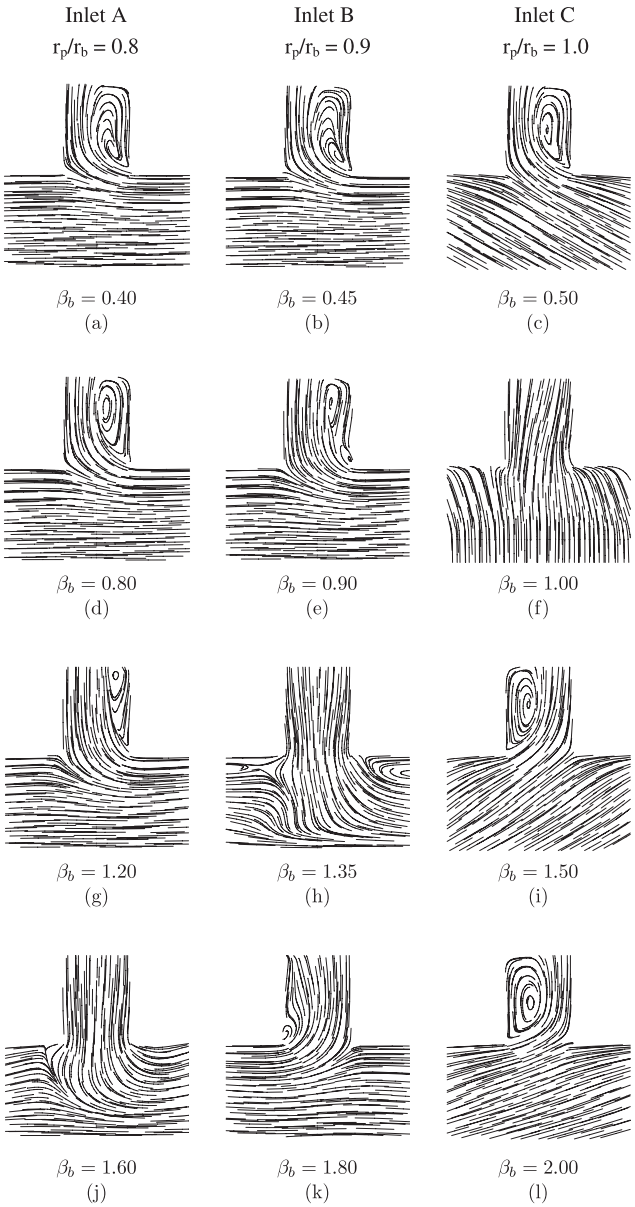


**Fig. 4** Computed flow structure in the tangential plane at the receiver hole radius, in a frame of reference rotating with the rotor (direction of motion from left to right), $\lambda_T = 0.24$

Figure 4 shows flow streamlines in the tangential ($\phi-$z) plane at the receiver hole radius $r_b$ in a frame of reference rotating at the speed of the rotor (in the left to right direction). In each image, the stator is at the bottom and the receiver hole and outlet are at the top. The three columns represent the three inlet positions, $r_p/r_b = 0.8$, 0.9, and 1.0, respectively, and the rows represent increasing values of preswirl ratio.

For $r_p/r_b = 0.8$, Fig. 4(a) shows a case for which $\beta_b = 0.40$ and is therefore 'under-swirled'. The receiver hole rotates more quickly than the flow in the core; therefore, the flow enters at an acute angle, separating at the leading edge of the hole, and causing a recirculation inside the hole. As the preswirl ratio is increased, the angle at which the flow enters the receiver hole tends towards the axial direction. At the point where synchronous rotation between the flow and the hole occurs, the flow would be expected to flow axially into the receiver hole, as can be seen in Fig. 4(j), for which $\beta_b = 1.6$.

As the inlet radius is increased, the inlet preswirl ratio required to produce this synchronous rotation is reduced. For $r_p/r_b = 0.9$, synchronous rotation occurs when $\beta_b = 1.35$ as shown in Fig. 4(h) and for $r_p/r_b = 1.0$, when $\beta_b = 1.0$ as shown in Fig. 4(f). When the swirl ratio is increased further, or 'over-swirled', the flow rotates more quickly than the receiver hole, causing separation and a region of recirculation at the trailing edge of the hole.

The variation of the swirl ratio $\beta = V_\phi/\Omega r$ midway between the rotor and stator ($z/s = 0.5$) and on a radial line midway between the receiver holes is shown in Fig. 5. Figures 5(a), (b), and (c) again correspond to the inlet at $r_p/r_b = 0.8$, 0.9, and 1.0, respectively. The horizontal axis is $1/x^2$, where $x = r/b$ is the non-dimensional radius.

In each case, a peak is seen in the swirl ratio at the inlet radius due to the high momentum inlet fluid. At higher radii (i.e. lower values of $x^{-2}$) there is a linear variation of $\beta$ with $x^{-2}$, consistent with free vortex behaviour. The dashed line on each plot is a least-squares best fit of the data in the linear region.

There is considerable uncertainty associated with the fit (especially as the region of linear behaviour becomes smaller); however, these results suggest that the flow is related to a Rankine (combined free and forced) vortex, for which

$$\beta = A + Bx^{-2} \tag{3}$$

where $A$ and $B$ are constants. This behaviour was found by Mirzaee *et al.* [**15**] to occur in a rotating cavity with a stationary outer casing.

Figure 6 shows the variation of swirl ratio in the core at the radius of the receiver hole, $\beta_\infty$, with the preswirl ratio at the inlet $\beta_b$. Each line represents a different inlet location and is approximately linear. Extrapolating back to the $\beta_b = 0$ condition, the value for $\beta_\infty$ would be expected to lie between 0.43, the value for turbulent flow in a sealed rotor–stator system (see Owen and Rogers [**10**]), and zero, due to the effect of a zero-swirl superposed flow on the swirl in the rotating core of fluid between the discs. It can be seen that a significant increase in inlet preswirl is required for the inlets at lower radii to achieve the synchronous rotation condition discussed above, and is illustrated by the horizontal dashed line in Fig. 6.

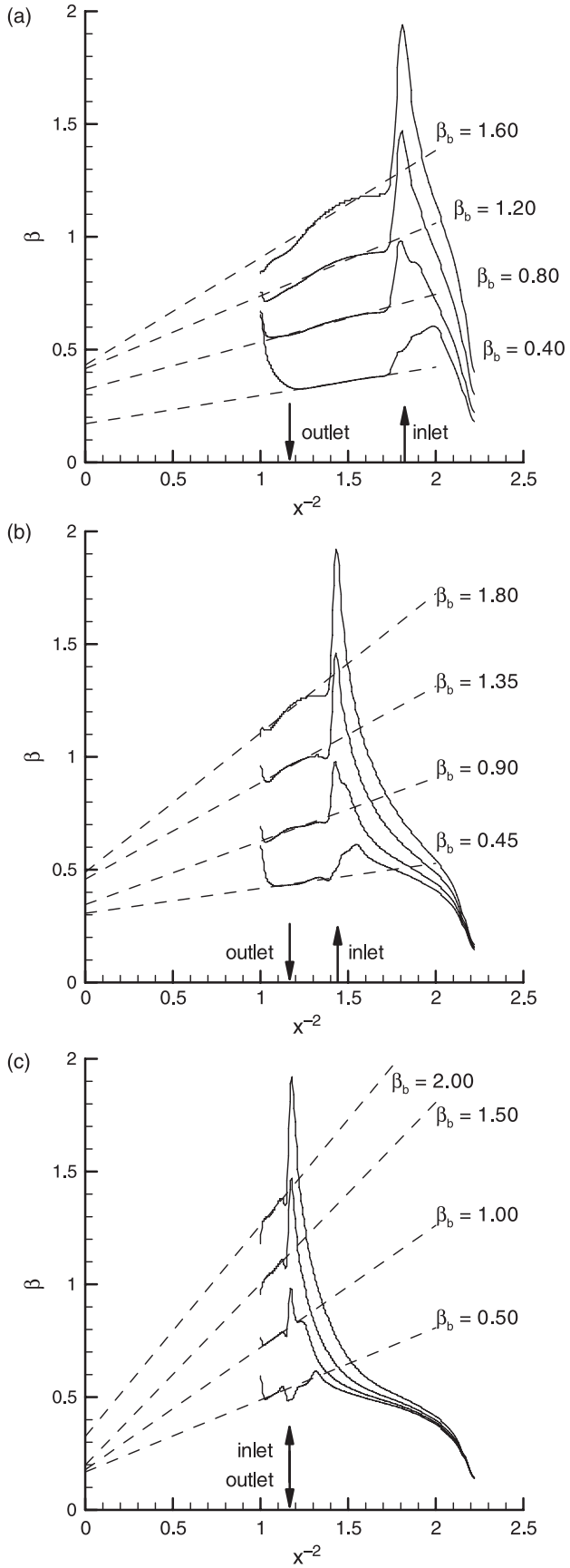


**Fig. 5** Computed tangential velocity distributions on the axial mid-plane: (a) $r_p/r_b = 0.8$, (b) $r_p/r_b = 0.9$, and (c) $r_p/r_b = 1.0$

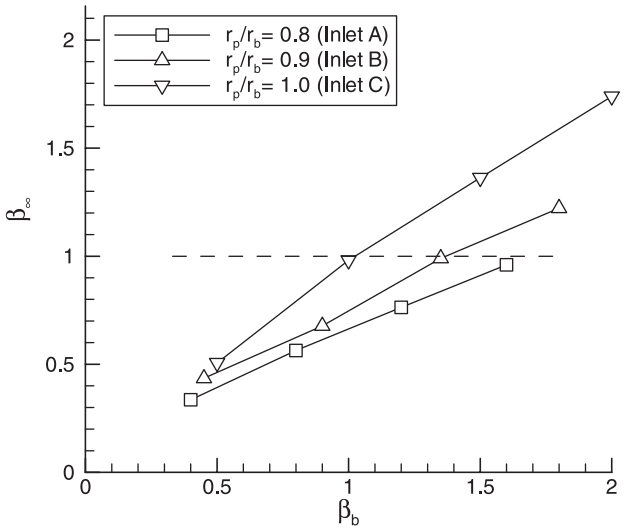


**Fig. 6** Computed variation of $\beta_\infty$ with $\beta_b$ for the three inlet locations, $\lambda_T = 0.24$

## 4 DISCHARGE COEFFICIENT

The discharge coefficient $C_{d,b}$ is defined here as the ratio of the actual mass flowrate through the receiver holes $\dot{m}_b$ to the isentropic mass flowrate $\dot{m}_i$ such that

$$C_{d,b} = \frac{\dot{m}_b}{\dot{m}_i} \tag{4}$$

The isentropic mass flowrate through the receiver holes was derived by Yan *et al.* [**7**] using the first law of thermodynamics for an adiabatic system, taking into account the work done by or on the fluid as it passes from station 1 in the fluid core to station 2 in the receiver holes. It is given by

$$\frac{\dot{m}_i}{A_b} = \rho_{0,1}\left(\frac{p_2}{p_{0,1}}\right)^{1/\gamma}\left\{\left(\frac{2\gamma}{\gamma-1}\right)\frac{p_{0,1}}{\rho_{0,1}}\left[1-\left(\frac{p_2}{p_{0,1}}\right)^{\gamma-1/\gamma}\right] + 2\Omega(r_2V_{\phi,2} - r_1V_{\phi,1}) - V_{\phi,2}^2\right\}^{1/2} \tag{5}$$

The first term inside the curly brackets is the standard result for compressible flow in a stationary nozzle; the second term is the work term resulting from the change of angular momentum of the air; the last term is due to the fact that the air in the receiver holes has an absolute tangential, as well as an axial, component of velocity. The derivation of equation (5) is given in Appendix 3. It should be noted that failure to use the correct equation for $\dot{m}_i$ can result in calculated values of $C_{d,b}$ exceeding unity, which is clearly nonsensical.

Figure 7 shows this discharge coefficient calculated using locations 1 and 2 as a point in the core at the radius of the receiver holes and the outlet plane, respectively. Figure 7(a), where $\beta_b$ is on the horizontal axis, clearly shows that to maximize the discharge

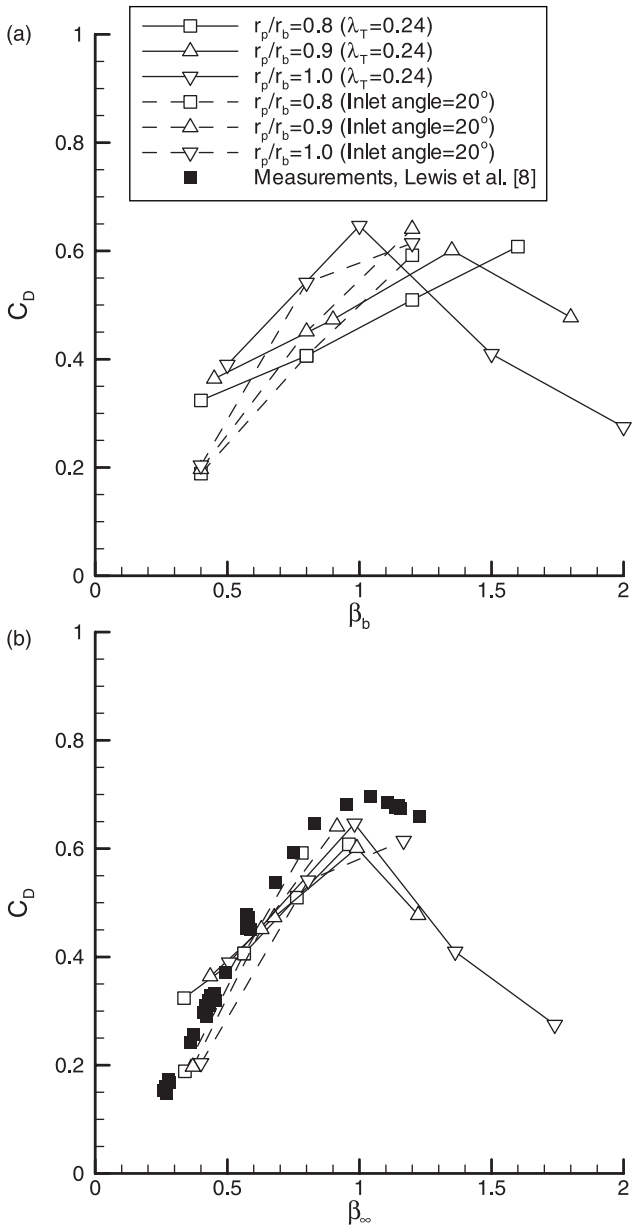


**Fig. 7** Computed variation of discharge coefficient $C_{d,b}$: with (a) $\beta_b$ and (b) $\beta_\infty$

coefficient for low radius inlets, the preswirl ratio must be greater than unity. The effect of varying preswirl ratio at a fixed non-dimensional flowrate $\lambda_T$ (the equivalent of physically altering the inlet preswirl angle) is to produce a sharp change in the relationship between $C_{d,b}$ and $\beta_b$ when the maximum value of $C_{d,b}$ is reached.

Lewis *et al.* [**8**] presented computations and measurements, for the $r_p/r_b = 0.8$ configuration also considered here, for a fixed inlet flow angle of 20° to the tangential in the direction of rotation of the disc and variable flowrate. In this case, the inlet preswirl ratio is proportional to the non-dimensional flowrate $\lambda_T$ used (at fixed $Re_\phi$). Results for computations at this same fixed inlet flow angle (for $0.12 < \lambda_T < 0.36$) are also shown in Fig. 7(a), and show a smaller effect of $r_p/r_b$ on the variation of $C_{d,b}$ with $\beta_b$. Figure 7(b) shows that, when the preswirl ratio is varied at a fixed value of $\lambda_T$, a nearly symmetric variation of $C_{d,b}$ around the point of synchronous rotation ($\beta_\infty = 1$) is obtained. (The values of inlet preswirl ratio $\beta_b$ required to achieve synchronous rotation at the receiver hole radius are discussed above in connection with Fig. 4.) There is reasonably good agreement between the computations and the measurements made by Lewis *et al.* for $r_p/r_b = 0.8$ and fixed inlet flow angle.

It was shown above that the effect of 'under-swirling' or 'over-swirling' the core body of fluid caused the flow to enter the receiver hole at an angle to the axial direction. This means that the effective area of the receiver hole, as 'seen' by the flow, is reduced. It is logical that, since the flowrate is proportional to the orifice area, $C_{d,b}$ will reduce linearly as the effective area is reduced.

The reduction in effective area $A_e$ can be expressed as a function of the flow angle at the receiver hole, shown in equation (6), where $\alpha$ is the flow angle measured from the axial direction

$$\frac{A_e}{A_b} = \cos\alpha \tag{6}$$

An equation can be formed for $\alpha$ by considering the ratio of the tangential velocity in the rotating frame and the axial velocity. The radial component of velocity is ignored as a large volume of the flow enters the hole from the core rather than from the boundary layer and therefore has very low radial velocity (see Lewis *et al.*'s discussion on 'direct' and 'indirect' routes). Hence

$$\tan\alpha = \frac{|V_{\phi,\infty} - \Omega r_b|}{V_{z,b}} \tag{7a}$$

where

$$V_{z,b} = \frac{\dot{m}_b}{\rho A_b} \tag{7b}$$

and

$$|V_{\phi,\infty} - \Omega r_b| = |\beta_\infty - 1|\Omega r_b \tag{7c}$$

Using the definition of $\lambda_T$ given in the nomenclature, it follows that

$$\frac{C_{d,b}}{C_{d,max}} = \frac{A_e}{A_b} = \frac{1}{\sqrt{1 + \left(\dfrac{A_b \rho |\beta_\infty - 1| \Omega r_b}{\mu b \lambda_T Re_\phi^{0.8}}\right)^2}} \tag{8}$$

where $C_{d,max}$ is the value of $C_{d,b}$ when $\beta_\infty = 1$.

Figure 8 shows $C_{d,b}/C_{d,max}$ for a range of conditions and flowrates. The model underpredicts the computational data, which suggests that the predicted flow angle is too large, so that the predicted effective area is

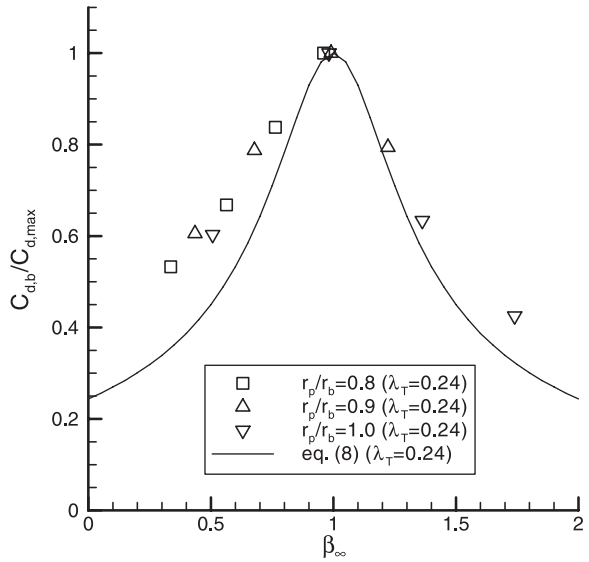


**Fig. 8** Variation of $C_{d,b}/C_{d,max}$ with $\beta_\infty$

too small. At the entrance to the hole, the circumferential velocity will be somewhere between that of the fluid in the core and that of the receiver hole.

Figure 9 shows the total pressure loss through the system, using the total pressure in the stationary frame at the inlet and in the rotating frame at the outlet. This difference is largely independent of flowrate. There is a significant increase in pressure loss as the preswirl ratio is increased. Figure 7(a) shows that the discharge coefficient for the receiver holes increases as the ratio $r_p/r_b$ increases; Fig. 9 shows, however, that increasing $r_p/r_b$ causes a slight increase in pressure drop.

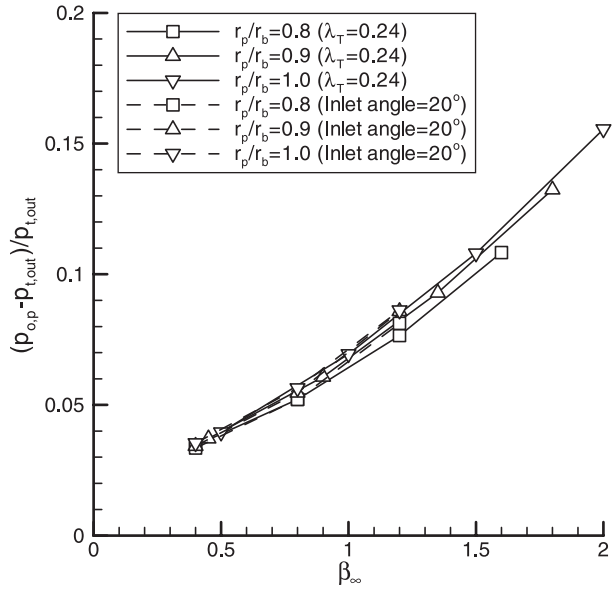


**Fig. 9** Computed variation of pressure drop from the preswirl inlet to the receiver-hole outlet with $\beta_b$

## 5 ADIABATIC EFFECTIVENESS

The adiabatic effectiveness $\Theta_{b,ad}$ is defined as the non-dimensional change in total temperature between the nozzles in the stationary frame and the receiver holes in the rotating frame

$$\Theta_{b,ad} = \frac{c_p(T_{o,p} - T_{t,b})}{1/2\Omega^2 r_b^2} \tag{9}$$

A theoretical value for $\Theta_{b,ad}$ was derived by Karabay *et al.* [**16**] for a cover-plate system using the first law of thermodynamics. The equivalent theoretical expression derived by Farzeneh-Gord *et al.* [**5**] for the direct-transfer system considered here is

$$\Theta_{b,ad} = 2\beta_p \left(\frac{r_p}{r_b}\right)^2 - 1 - \frac{M_s}{1/2\dot{m}\Omega r_b^2} \tag{10}$$

When expressed in terms of $\beta_b$, the preswirl ratio based on the receiver-hole radius, this relationship becomes

$$\Theta_{b,ad} = 2\beta_b \frac{r_p}{r_b} - 1 - \frac{M_s}{1/2\dot{m}\Omega r_b^2} \tag{11}$$

Figure 10 shows the computed effectiveness plotted against the relationship in equation (11). Note that a computed moment on the stator is necessary to evaluate the relationship and hence only discrete values are available. The agreement between the two is excellent. As shown in the Appendix 2, in practice the increase of $\Theta_{b,ad}$ with increasing $r_p$ will be less than that shown in Fig. 10.

For turbine blade cooling, the effectiveness should be as high as possible as this ensures that the fluid reaching the blades has the lowest possible total temperature. In general, configurations with low preswirl

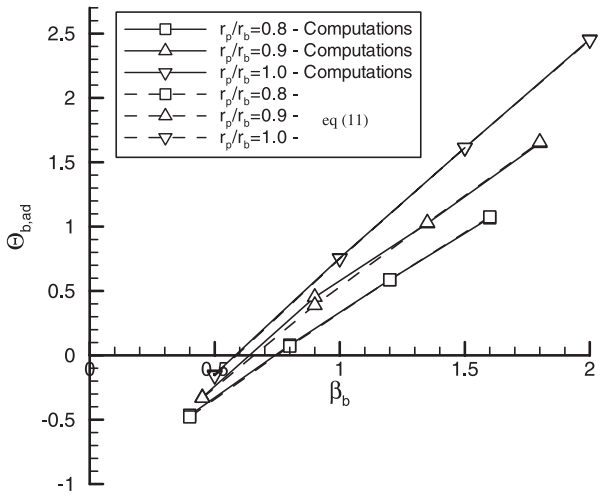


**Fig. 10** Computed variation of adiabatic effectiveness $\Theta_{b,ad}$ with $\beta_b$

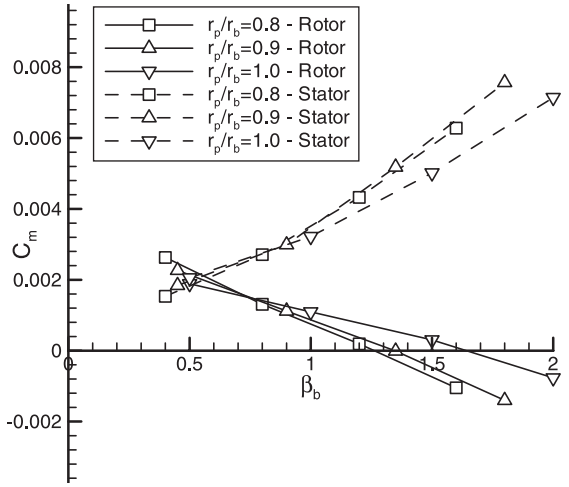


**Fig. 11** Computed values of moment coefficient $C_M$ on the rotor and the stator, $\lambda_T = 0.24$

ratios require work to be performed on the flow by the rotor to bring its tangential velocity to that of the receiver holes, and this work input raises the total temperature of the flow. Conversely, configurations with high preswirl ratios perform work on the rotor, thus reducing the total temperature.

As shown in equation (11), the relationship between the preswirl ratio and the adiabatic effectiveness is approximately linear, with the gradient dependent on $r_p/r_b$. As the radius of the inlet increases, there is consequently a resulting increase in effectiveness.

A secondary effect adding to the improvement in effectiveness for high radius inlets is the reduction in moment on the stator. This is shown in Fig. 11; as the preswirl ratio is increased, the moment on the stator increases and that on the rotor decreases. The change in moment coefficient is slightly less for $r_p/r_b = 1$ than that for the other two locations.

## 6 CONCLUSIONS

The effect of nozzle location on the fluid dynamics of a preswirl system has been studied computationally. The model, which has been validated previously using an experimental rig at the University of Bath, produces a flow structure representative of that found in gas turbine engines. Computations were performed at $Re_\phi = 10^6$, $0.12 < \lambda_T < 0.36$, and $0.5 < \beta_b < 2.0$.

The main conclusions from the study are as follows.

1. $C_{d,b}$, the discharge coefficient for the receiver holes, is maximized when the core flow is in synchronous rotation with the holes ($\beta_\infty = 1$).
2. A simple model based on the effective receiver-hole area can be used to estimate the reduction in $C_{d,b}$ when $\beta_\infty \neq 1$.
3. The maximum $C_{d,b}$ is achieved at a value of $\beta_b$ that decreases as $r_p/r_b$ increases, with a corresponding slight increase in the pressure drop in the system.
4. The adiabatic effectiveness increases as $r_p/r_b$ increases, and computed values are in excellent agreement with the theoretical analysis.

As shown in Appendix 2, the variation of static pressure in the core will reduce, but will not negate, the advantages of locating the preswirl nozzles at as high a radius as practicable. It is also shown in Appendix 2 that the increase in effectiveness as $r_p$ increases is caused solely by losses in the nozzles and in the core.

## ACKNOWLEDGEMENT

The Engineering and Physical Sciences Research Council (EPSRC) sponsored Paul Lewis's research at the University of Bath through Doctoral Training Account EP/P500036/1.

## REFERENCES

1 **Meierhofer, B.** and **Franklin, C. J.** An investigation of a preswirled cooling airflow to a turbine disc by measuring the air temperature in the rotating channels. ASME paper 81-GT-132, 1981.
2 **Wilson, M., Pilbrow, R.,** and **Owen, J. M.** Flow and heat transfer in a pre-swirl rotor–stator system. *ASME J. Turbomach.*, 1997, **119**, 364–373.
3 **Geis, T., Dittmann, M.,** and **Dullenkopf, K.** Cooling air temperature reduction in a direct transfer preswirl system. *J. Eng. Gas Turbines Power*, 2004, **126**, 809–815.
4 **Chew, J. W., Ciampoli, F., Hills, N. J.,** and **Scanlon, T.** Preswirled cooling air delivery system performance. ASME paper GT2005-68323, 2005.
5 **Farzaneh-Gord, M., Wilson, M.,** and **Owen, J. M.** Numerical and theoretical study of flow and heat transfer in a pre-swirl rotor–stator system. ASME paper GT2005-68135, 2005.
6 **Dittmann, M., Geis, T., Schramm, V., Kim, S.,** and **Wittig, S.** Discharge coefficients of a preswirl system in secondary air systems. *ASME J. Turbomach.*, 2002, **124**, 119–124.
7 **Yan, Y., Farzaneh-Gord, M., Lock, G., Wilson, M.,** and **Owen, J. M.** Fluid dynamics of a pre-swirl rotor–stator system. *ASME J. Turbomach.*, 2003, **125**, 641–647.
8 **Lewis, P., Wilson, M., Lock, G. D.,** and **Owen, J.** Physical interpretation of flow and heat transfer in pre-swirl systems. *J. Eng. Gas Turbines Power*, 2007, **129**, 769–777.
9 **Jarzombek, K., Benra, F.-K., Dohmen, H. J.,** and **Schneider, O.** CFD analysis of flow in high-radius preswirl systems. ASME paper GT2007-27404, 2007.
10 **Owen, J. M.** and **Rogers, R. H.** *Flow and heat transfer in rotating-disc systems*; *Rotor–stator systems*, 1989, vol. 1 (Research Studies Press, Taunton, UK).
11 **Barth, T. J.** and **Jesperson, D. C.** The design and application of upwind schemes on unstructured meshes. AIAA paper 89-0366, 1989.

**12 Menter, F. R.** Two-equation eddy viscosity turbulence models for engineering applications. *AIAA J.*, 1994, **32**, 269–289.

**13 Wilcox, D. C.** *Turbulence modelling for CFD*, 2nd edition, 1998 (DCW Industries, La Canada, CA).

**14 Evans, J., Stevens, L. M., Bodily, C.,** and **Kang, M.-K. B.** Prediction of velocities and heat transfer coefficients in a rotor-stator cavity. ASME paper GT2004-53639, 2004.

**15 Mirzaee, I., Gan, X., Wilson, M.,** and **Owen, J. M.** Heat transfer in a rotating cavity with a peripheral inflow and outflow of cooling air. *ASME J. Turbomach.*, 1998, **120**, 818–823.

**16 Karabay, H., Wilson, M.,** and **Owen, J. M.** Predictions of effect of swirl on flow and heat transfer in a rotating cavity. *Int. J. Heat Fluid Flow*, 2001, **22**, 143–155.


## APPENDIX 1

### Notation

| | |
|---|---|
| $a, b$ | rotor inner radius, rotor outer radius |
| $A, B$ | combined free and forced vortex coefficients |
| $A_b$ | receiver hole area |
| $c_p$ | specific heat capacity at constant pressure |
| $c_w$ | non-dimensional mass flowrate ($=\dot{m}/\mu b$) |
| $C_d$ | discharge coefficient (equation (4) or (12)) |
| $C_M$ | disc moment coefficient ($=M/(1/2)\rho\Omega^2 b^5$) |
| $G$ | gap ratio ($=s/b$) |
| $\dot{m}$ | mass flowrate |
| $M$ | moment on one side of the disc |
| $r$ | radius |
| $r_p, r_b$ | radii of preswirl nozzles and receiver holes |
| $Re_\phi$ | rotational Reynolds number ($=\rho\Omega b^2/\mu$) |
| $s$ | rotor–stator separation distance |
| $T$ | temperature |
| $V$ | velocity |
| $x$ | non-dimensional radius ($=r/b$) |
| $\alpha$ | flow angle relative to the axial direction |
| $\beta$ | swirl ratio ($=V_\phi/\Omega r$) |
| $\beta_b$ | preswirl ratio based on $r_b$($=V_{\phi,p}/\Omega r_b$) |
| $\beta_p$ | preswirl ratio based on $r_p$($=V_{\phi,p}/\Omega r_p$) |
| $\gamma$ | ratio of specific heats |
| $\theta$ | inlet nozzle angle to the tangential direction |
| $\Theta_{b,ad}$ | adiabatic effectiveness ($c_p(T_{o,p}-T_{t,b})/(1/2)\Omega^2 r_b^2$) |
| $\lambda_T$ | turbulent flow parameter ($=c_w Re_\phi^{-0.8}$) |
| $\mu$ | dynamic viscosity |
| $\rho$ | density |
| $\Omega$ | angular velocity of the rotor |

*Subscripts*

| | |
|---|---|
| ad | adiabatic |
| b | blade-cooling |
| e | effective |
| i | isentropic value |
| max | maxium value |
| o | total value in the stationary frame |
| out | at the receiver hole outlet |
| p | preswirl |
| s | stator |
| t | total value in the rotating frame |
| $w$ | rotor |
| $\phi, r, z$ | circumferential, radial, and axial direction |
| $\infty$ | value in core at $z/s=0.5$, $r/r_b=1$ |
| 1,2 | upstream, downstream locations in the streamtube |

## APPENDIX 2

### Effect of core swirl on preswirl ratio

If $V_T$ is the total velocity leaving the nozzles, then for *incompressible flow*

$$V_T = C_{d,p}\left[\frac{2(p_0-p_p)}{\rho}\right]^{1/2} \tag{12}$$

where $p_0$ is the total pressure upstream of the nozzles, $p_p$ is the static pressure in the core at the radius of the nozzles, and $C_{d,p}$ is the discharge coefficient for the nozzles, and

$$V_T = \frac{V_{\phi,p}}{\cos\theta} = \frac{\beta_b \Omega r_b}{\cos\theta} \tag{13}$$

$\theta$ being the nozzle angle to the tangential direction. Hence

$$\beta_b = \frac{C_{d,p}\cos\theta}{\Omega\, r_b}\left[\frac{2\,(p_0-p_p)}{\rho}\right]^{1/2} \tag{14}$$

If $\beta_{b,1}$ is the value of $\beta_b$ when $r_p/r_b=1$, it follows that

$$\beta_{b,1} = \frac{C_{d,p}\cos\theta}{\Omega\, r_b}\left[\frac{2\,(p_0-p_b)}{\rho}\right]^{1/2} \tag{15}$$

and hence

$$\frac{\beta_b}{\beta_{b,1}} = \left[1-\frac{C_{d,p}^2\cos^2\theta(p_b-p_p)}{1/2\rho\beta_b^2\Omega^2 r_b^2}\right]^{-1/2} \tag{16}$$

Consider a combined vortex in the core, as shown in Fig. 5, where

$$\frac{V_\phi}{\Omega r} = A + B\left(\frac{r}{b}\right)^{-2} \tag{17}$$

It follows that

$$\frac{\mathrm{d}p}{\mathrm{d}r} = \rho\frac{V_\phi^2}{r} = \rho\Omega^2 r\left[A^2 + 2AB\left(\frac{r}{b}\right)^{-2} + B^2\left(\frac{r}{b}\right)^{-4}\right] \tag{18}$$

Integrating from $r = r_p$ to $r = r_b$

$$p_b - p_p = \frac{1}{2}\rho\Omega^2 r_b^2 \times \left\{ A^2 \left(1 - \frac{r_p^2}{r_b^2}\right) - 4AB\left(\frac{r_b}{b}\right)^{-2} \times \ln\left(\frac{r_p}{r_b}\right) + B^2\left(\frac{r_b}{b}\right)^{-4}\left[\left(\frac{r_p}{r_b}\right)^{-2} - 1\right]\right\} \tag{19}$$

and from equation (16)

$$\frac{\beta_b}{\beta_{b,1}} = \left\{1 - \frac{C_{d,p}^2 \cos^2\theta}{\beta_b^2} \times \left[A^2\left(1 - \frac{r_p^2}{r_b^2}\right) - 4AB\left(\frac{r_b}{b}\right)^{-2}\ln\left(\frac{r_p}{r_b}\right) + B^2\left(\frac{r_b}{b}\right)^{-4} \times \left(\left(\frac{r_p}{r_b}\right)^{-2} - 1\right)\right]\right\}^{-1/2} \tag{20}$$

The results corresponding to Fig. 5 are shown in Table 1 for an assumed value of $C_{d,p} = 0.9$ and $\theta = 20°$, which corresponds to the nozzle angle in the experimental rig.

Consider the *ideal case* where $C_{d,p} = 1$, $\theta = 0$, and free-vortex flow occurs in the core, such that $A = 0$ and

$$\frac{V_\phi}{\Omega r} = B\left(\frac{r}{b}\right)^{-2} \tag{21}$$

It follows that

$$\frac{V_{\phi,p}}{\Omega r_p} = B\left(\frac{r_p}{b}\right)^{-2} \tag{22}$$

and

$$\beta_b = \frac{V_{\phi,p}}{\Omega r_b} = B\left(\frac{r_p r_b}{b^2}\right)^{-1} \tag{23}$$

Hence

$$B = \beta_b \frac{r_p r_b}{b^2} \tag{24}$$

and equation (20) reduces to

$$\frac{\beta_b}{\beta_{b,1}} = \frac{r_b}{r_p} \tag{25}$$

Reference to equation (11) shows that for this ideal case (where $\beta_b r_p / r_b$ is constant) the nozzle location has no effect on the adiabatic effectiveness! However, Table 1 shows that for the real case, although the core swirl reduces the advantage, the effectiveness increases as $r_p$ increases. *It can therefore be concluded that the increase in effectiveness as $r_p$ increases is caused solely by losses in the nozzles and in the core.*

## APPENDIX 3

### Discharge coefficient for holes in a rotating disc

Referring to Fig. 12, air leaves station 1 at the exit from preswirl nozzles, with resultant speed $U_1$, in a stationary frame of reference, where

$$U_1^2 = V_{r_1}^2 + V_{\phi_1}^2 + V_{z_1}^2 \tag{26}$$

$V_r$, $V_\phi$, and $V_z$ being the radial, tangential, and axial components of velocity in a stationary frame of reference, and

$$V_{\phi_1} = \beta_p \Omega r_1 \tag{27}$$

$\beta_p$ being the preswirl ratio.

Air enters the axial receiver holes in the rotating disc with resultant speed $U_2$, in a stationary frame, where

$$U_2^2 = V_{\phi_2}^2 + V_{z_2}^2 \tag{28}$$

and the radial component, $V_{r_2}$, is taken to be zero. If the air achieves solid-body rotation in the receiver holes,

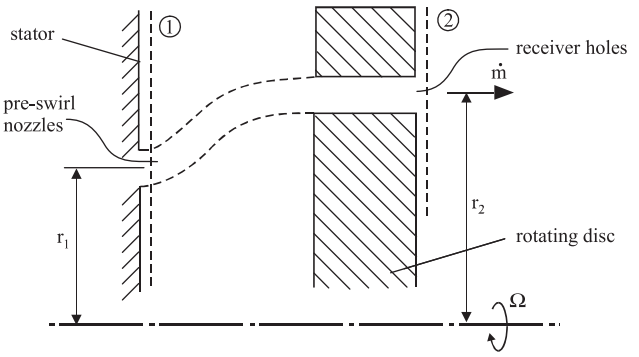


**Fig. 12** Streamtube for derivation of isentropic mass flowrate

**Table 1** Effect of core swirl on $\beta_b/\beta_{b,1}$ according to equation (20) with $\theta = 20°$ and $C_{d,p} = 0.9$

| $r_p/r_b$ | 0.8 | | | | 0.9 | | | |
|---|---|---|---|---|---|---|---|---|
| $\beta_b$ | 0.40 | 0.80 | 1.20 | 1.60 | 0.45 | 0.90 | 1.35 | 1.80 |
| $A$ | 0.17 | 0.32 | 0.42 | 0.43 | 0.31 | 0.35 | 0.46 | 0.49 |
| $B$ | 0.13 | 0.21 | 0.32 | 0.48 | 0.11 | 0.28 | 0.43 | 0.62 |
| $\beta_b/\beta_{b,1}$ | 1.12 | 1.09 | 1.08 | 1.07 | 1.08 | 1.05 | 1.04 | 1.04 |

then

$$V_{\phi_2} = \Omega r_2 \tag{29}$$

but this is not necessarily the case in practice.

Define the discharge coefficient, $C_D$, for the receiver holes as

$$C_D = \frac{\dot{m}}{\dot{m}_i} \tag{30}$$

where $\dot{m}$ is the actual mass flowrate and $\dot{m}_i$ is the isentropic value.

Consider isentropic flow from 1 to 2, where the work done by the air, $\dot{W}_{12}$, is given by

$$-\frac{\dot{W}_{12}}{\dot{m}} = \Omega(r_2 V_{\phi,2} - r_1 V_{\phi,1}) = c_p(T_{0,2} - T_{0,1}) \tag{31}$$

where $T_0$, the total temperature in a *stationary* frame, is

$$c_p T_0 = c_p T + \frac{1}{2}U^2 \tag{32}$$

$T$ being the static temperature.

Now for isentropic flow

$$\frac{p}{\rho^\gamma} = \text{constant} \tag{33}$$

and

$$\rho_2 = \rho_{0,1}\left(\frac{p_2}{p_{0,1}}\right)^{1/\gamma} \tag{34}$$

Also, for a perfect gas

$$R = c_p\frac{\gamma - 1}{\gamma} \tag{35}$$

Hence

$$c_p(T_{0,2} - T_{0,1}) = \frac{\gamma}{\gamma - 1}\frac{p_{0,1}}{\rho_{0,1}}\left[\left(\frac{p_2}{p_{0,1}}\right)^{\gamma-1/\gamma} - 1\right] + \frac{1}{2}U_2^2 \tag{36}$$

Equation (31) subsequently becomes

$$\frac{\gamma}{\gamma - 1}\frac{p_{0,1}}{\rho_{0,1}}\left[\left(\frac{p_2}{p_{0,1}}\right)^{\gamma-1/\gamma} - 1\right] + \frac{1}{2}\left(V_{\phi,2}^2 + V_{z,2}^2\right) = \Omega\left(r_2 V_{\phi,2} - r_1 V_{\phi,1}\right) \tag{37}$$

Hence

$$V_{z,2} = \left\{\left(\frac{2\gamma}{\gamma - 1}\right)\frac{p_{0,1}}{\rho_{0,1}}\left[1 - \left(\frac{p_2}{p_{0,1}}\right)^{\gamma-1/\gamma}\right] + 2\Omega\left(r_2 V_{\phi,2} - r_1 V_{\phi,1}\right) - V_{\phi,2}^2\right\}^{1/2} \tag{38}$$

Now

$$\dot{m}_i = \rho_2 A_2 V_{z,2} \tag{39}$$

where $A_2$ is the area of the receiver holes. Hence, using equations (34) and (38)

$$\frac{\dot{m}_i}{A_2} = \rho_{0,1}\left(\frac{p_2}{p_{0,1}}\right)^{1/\gamma}\left\{\frac{2\gamma}{\gamma - 1}\frac{p_{01}}{\rho_{0,1}}\left[1 - \left(\frac{p_2}{p_{0,1}}\right)^{\gamma-1/\gamma}\right] + 2\Omega\left(r_2 V_{\phi,2} - r_1 V_{\phi,1}\right) - V_{\phi,2}^2\right\}^{1/2} \tag{40}$$

This is equation (5) in the article.

If $V_{\phi,1} = V_{\phi,2} = 0$, then equation (15) becomes

$$\frac{\dot{m}_i}{A_2} = \left\{\frac{2\gamma}{\gamma - 1}p_{0,1}\,\rho_{0,1}\left(\frac{p_2}{p_{0,1}}\right)^{2/\gamma}\left[1 - \left(\frac{p_2}{p_{0,1}}\right)^{\gamma}\right]\right\}^{1/2} \tag{41}$$

which is the standard result for a stationary nozzle.

Alternatively, if solid-body rotation is achieved in the receiver holes such that

$$V_{\phi,2} = \Omega r_2 \tag{42}$$

Then with the preswirl ratio, $\beta_p$, is defined as

$$\beta_p = \frac{V_{\phi,1}}{\Omega r_1} \tag{43}$$

Equation (40) becomes

$$\frac{\dot{m}_i}{A_2} = \rho_{0,1}\left(\frac{p_2}{p_{0,1}}\right)^{1/\gamma}\left\{\frac{2\gamma}{\gamma - 1}\frac{p_{0,1}}{\rho_{0,1}}\left[1 - \left(\frac{p_2}{p_{0,1}}\right)^{\gamma-1/\gamma}\right] + \Omega^2 r_2^2\left[1 - 2\beta_p\left(\frac{r_1}{r_2}\right)^2\right]\right\}^{1/2} \tag{44}$$

This is appropriate for long receiver holes or for a gas turbine disc in which the air achieves solid-body rotation. (In principle, solid-body rotation can be achieved without friction – e.g. using radial vanes, as in a compressor – and the process could still be treated as

isentropic.) For this case, if $\beta_p(r_1/r_2)^2 < 1/2$ then $\dot{m}_i$ is greater than that for the zero-swirl case given by equation (41). Thus, if $C_D$ defined in equation (30) were based on equation (41), it would be possible that $C_D > 1$, an undesirable result.

Some authors have expressed $\dot{m}_i$ in terms of relative total pressures. This is equivalent to using equation (41) with $p_{0,1}$ and $\rho_{0,1}$ replaced by relative values (i.e. values referred to a rotating frame of reference). This is based on the assumption that

$$T_{0,2,rel} = T_{0,1,rel} \tag{45}$$

where

$$c_p T_{0,rel} = c_p T + \frac{1}{2}\left[V_r^2 + V_z^2 + \left(\Omega r - V_\phi\right)^2\right] \tag{46}$$

$(\Omega r - V_\phi)$ being the tangential component of velocity in a rotating frame of reference.

Equation (46) can be written as

$$c_p T_{0,rel} = c_p T + \frac{1}{2}\left(V_r^2 + V_\phi^2 + V_z^2\right) + \frac{1}{2}\Omega^2 r^2 - \Omega r V_\phi \tag{47}$$

$$= c_p T_0 + \frac{1}{2}\Omega^2 r^2 - \Omega r V_\phi \tag{48}$$

Hence

$$c_p(T_{0,2,rel} - T_{0,1,rel}) = c_p(T_{0,2} - T_{0,1}) - \Omega(r_2 V_{\phi,2} - r_1 V_{\phi,1} + \frac{1}{2}\Omega(r_2^2 - r_1^2) \tag{49}$$

Referring to equation (31) it follows that, for isentropic flow

$$c_p(T_{0,2,rel} - T_{0,1,rel})\frac{1}{2}\Omega(r_2^2 - r_1^2) \tag{50}$$

which is only zero when $r_1 = r_2$. In other cases, the assumption in equation (45) is invalid.